Dimensional Analysis of Natural Vibrations of Planar Multilink Flexible Robots with Elastic Constraints at Actuator Gearhead Shaft–Link Couplings

Francis Kunzi Tekweme
Department of Mechanical and Industrial Engineering
University of Johannesburg
Johannesburg, RSA
ftekweme@uj.ac.za

Abstract

Non-dimensional variables are very useful as they reduce the number of variables when analyzing physical phenomenon. In this paper, the solutions to the frequency equation of multilink flexible robots with elastic constraints is analyzed in a compact form using the dimensional analysis. First, dimensionless governing differential equation of motion is presented. Second, dimensionless boundary conditions are obtained. Third, the dimensionless frequency equation and the orthogonality conditions among the mode shapes are derived. Fourth, some degenerate cases are developed and compared against some existing models. Finally, dimensionless wave numbers are plotted for various joint stiffness ratio to show the influence of various dimensionless parameters on the natural vibrational behavior of the planar multilink flexible robots.

Keywords
Dimensionless, planar, mode, vibration, wave.

1. Introduction
Most studies dealing with the vibrational behavior of planar multilink flexible robots have considered the base of each link as clamped to the actuator gearhead shaft. Such approaches however failed to consider the relative displacement between link and actuator shaft. Beards (1995) observed that actual connections have always some degree of flexibility. Moreover, few previous published studies focus on the dimensional analysis of the multilink flexible robots. However, dimensionless analysis reduces the number of relevant variables needed to describe a physical phenomenon (Volker, Bernhard & Hassan, 2017). Han, Benaroya and Wei (1999) investigated the dynamics of transversely vibrating beams using dimensionless quantities. The aim of this paper is to conduct a dimensional analysis of natural vibrations of planar multilink flexible robots with elastic constraints focusing on the dimensionless wave numbers.

1. Equation of motion and boundary conditions
Consider a planar multilink flexible robot with link i connected to the shaft of the gearhead of the ith actuator. The link- shaft connection can be modelled as either clamped or elastic. Figure 1 represents the traditional clamped model against the elastic constraint model.

© IEOM Society International

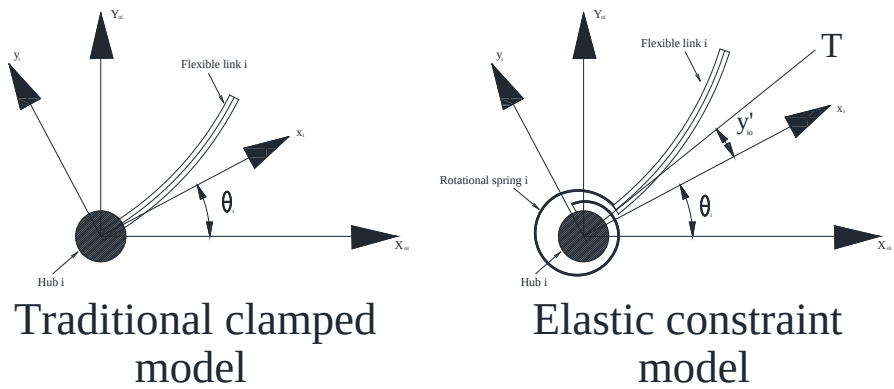

Figure 1. Traditional clamped and elastic constraint models of planar multilink flexible robots.
The governing differential equation of motion of Euler Bernoulli beam is given by

$$(EI)_i \frac{\partial^4 y_i(x_i, t)}{\partial x_i^4} + \rho_i \frac{\partial^2 y_i(x_i, t)}{\partial t^2} = 0 \tag{1}$$

where $y_i(x_i, t)$ is the link i transverse deflection at abscissa x_i and time t, I_i is the area moment of inertia of link i about the neutral axis, E_i is the modulus of elasticity of link i and ρ_i is the linear density of link i.
The length scales are non- dimensionalized by the length of the beam as follows

$$L_i = \frac{l_i}{l_i} = 1, \qquad X_i = \frac{x_i}{l_i}, \qquad Y_i = \frac{y_i}{l_i} \tag{2}$$

The time scale is non- dimensionalized by τ as follows

$$\tau = l_i^2 \sqrt{\frac{\rho_i}{(EI)_i}}, \qquad T = \frac{t}{\tau} \tag{3}$$

Substituting (2) and (3) into (1), the dimensionless governing equation of motion of Euler Bernoulli beam is given by

$$\frac{\partial^4 Y_i(X_i, T)}{\partial X_i^4} + \frac{\partial^2 Y_i(X_i, T)}{\partial T^2} = 0 \tag{4}$$

The boundary conditions for planar multilink flexible robot with rotational constraint is given by

$$y_i(x_i, t)|_{x_i=0} = 0 \tag{5}$$

$$(EI)_i \left.\frac{\partial^2 y_i(x_i, t)}{\partial x_i^2}\right|_{x_i=0} = \sigma_{oti} \left(\left.\frac{\partial y_i(x_i, t)}{\partial x_i}\right|_{x_i=0} \right) \tag{6}$$

$$(EI)_i \left.\frac{\partial^2 y_i(x_i, t)}{\partial x_i^2}\right|_{x_i=l_i} = -J_{Li} \frac{d^2}{dt^2} \left(\left.\frac{\partial y_i(x_i, t)}{\partial x_i}\right|_{x_i=l_i} \right) - (MD)_i \frac{d^2}{dt^2} \left(y_i(x_i, t)|_{x_i=l_i} \right) \tag{7}$$

$$(EI)_i \left.\frac{\partial^3 y_i(x_i, t)}{\partial x_i^3}\right|_{x_i=l_i} = M_{Li} \frac{d^2}{dt^2} \left(y_i(x_i, t)|_{x_i=l_i} \right) + (MD)_i \frac{d^2}{dt^2} \left(\left.\frac{\partial y_i(x_i, t)}{\partial x_i}\right|_{x_i=l_i} \right) \tag{8}$$

where σ_{oti} is the spring rotational stiffness for joint i, J_{Li} is the actual moment of inertia at the distal end of link i, M_{Li} is the actual mass at the distal end of link i and $(MD)_i$ is the contribution of masses non-collocated at the distal end of link i.
The dimensionless stiffness of joint *i* (K_{oi}) is defined in terms of the rotational spring stiffness and link *i* flexural rigidity as follows (McGuire, 1995)

$$K_{oi} = \frac{\sigma_{oti} l_i}{(EI)_i} \tag{9}$$

The dimensionless actual moment of inertia at the distal end of link *i* is given by

$$\Gamma_{Li} = \frac{J_{Li}}{\rho_i l_i^3} \tag{10}$$

The dimensionless contribution of masses non-collocated at the distal end of link i is given by

$$\mu_{di} = \frac{(MD)_i}{\rho_i l_i^2} \tag{11}$$

The dimensionless actual mass at the distal end of link i defined as follows

$$\Lambda_{Li} = \frac{M_{Li}}{\rho_i l_i} \tag{12}$$

The dimensionless boundary conditions for planar multilink flexible robot with rotational constraint are defined in terms of dimensionless parameters as follows:

$$Y_i(X_i,T)|_{X_i=0} = 0 \tag{13}$$

$$\left.\frac{\partial^2 Y_i(X_i,T)}{\partial X_i^2}\right|_{X_i=0} = K_{oi}\left.\frac{\partial Y_i(X_i,T)}{\partial X_i}\right|_{X_i=0} \tag{14}$$

$$\left.\frac{\partial^2 Y_i(X_i,T)}{\partial X_i^2}\right|_{X_i=1} = -\Gamma_{Li}\frac{\partial^2}{\partial T^2}\left[\left.\frac{\partial Y_i(X_i,T)}{\partial X_i}\right|_{X_i=1}\right] - \mu_{di}\frac{\partial^2}{\partial T^2}\left[Y_i(X_i,T)|_{X_i=1}\right] \tag{15}$$

$$\left.\frac{\partial^3 Y_i(X_i,T)}{\partial T^3}\right|_{X_i=1} = \Lambda_{Li}\frac{\partial^2}{\partial T^2}\left[Y_i(X_i,T)|_{X_i=1}\right] + \mu_{di}\frac{\partial^2}{\partial T^2}\left[\left.\frac{\partial Y_i(X_i,T)}{\partial X_i}\right|_{X_i=1}\right] \tag{16}$$

The general solution of the dimensionless governing differential equation (4) can be expressed as follows:

$$Y_i(X_i,T) = \Phi_i(X_i)\Theta(T) \tag{17}$$

Substituting (17) into (4) results in the following two separate differential equations:

$$\frac{d^4\Phi_i(X_i)}{dX_i^4} - \omega_i^2\Phi_i(X_i) = 0$$

$$\frac{d^2\Theta(T)}{dT^2} + \omega_i^2\Theta(T) = 0 \tag{19}$$

The solution to differential equation (18) can be written as follows:

$$\Phi_i(X_i) = C_{1i}\cos a_i X_i + C_{2i}\sin a_i X_i + C_{3i}\cosh a_i X_i + C_{4i}\sinh a_i X_i \tag{20}$$

where

$a_i = \sqrt{\omega_i}$ is the dimensionless wave number (21)

2. General Frequency equation and Orthogonality Conditions

The general frequency equation is derived by writing a set of homogeneous equations in three unknown constants C_{1i}, C_{2i} and C_{4i}, and setting to zero the determinant of the coefficient matrix.
Substituting (20) into (17), and then in (13) yields

$$C_{1i} = -C_{3i} \tag{22}$$

Plugging (22) into (20) gives

$$\Phi_i(X_i) = C_{1i}[\cos a_i X_i - \cosh a_i X_i] + C_{2i} \sin a_i X_i + C_{4i} \sinh a_i \; X_i \tag{23}$$

Substituting (23) into (17), and then in (14) through (16) yields a set of three homogeneous equations

$$\begin{bmatrix} F_{11} & F_{12} & F_{13} \\ F_{21} & F_{22} & F_{23} \\ F_{31} & F_{32} & F_{33} \end{bmatrix} \begin{bmatrix} C_{1i} \\ C_{2i} \\ C_{4i} \end{bmatrix} = \begin{bmatrix} 0 \\ 0 \\ 0 \end{bmatrix} \tag{24}$$

where

$$\begin{aligned}
F_{11} &= -2a_i \\
F_{12} &= -K_{oi} \\
F_{13} &= -K_{oi} \\
F_{21} &= -\cos a_i - \cosh a_i + \Gamma_{Li} a_i^3 [\sin a_i + \sinh a_i] - \mu_{di} a_i^2 [\cos a_i - \cosh a_i] \\
F_{22} &= -\sin a_i - \Gamma_{Li} a_i^3 \cos a_i - \mu_{di} a_i^2 \sin a_i \\
F_{23} &= \sinh a_i - \Gamma_{Li} a_i^3 \cosh a_i - \mu_{di} a_i^2 \sinh a_i \\
F_{31} &= \sin a_i - \sinh a_i + \Lambda_{Li} a_i [\cos a_i - \cosh a_i] + \mu_{di} a_i^2 [-\sin a_i - \sinh a_i] \\
F_{32} &= -\cos a_i + \Lambda_{Li} a_i \sin a_i + \mu_{di} a_i^2 \cos a_i \\
F_{33} &= \cosh a_i + \Lambda_{Li} a_i \sinh a_i + \mu_{di} a_i^2 \cosh a_i
\end{aligned}$$

Setting to zero the determinant of the coefficients matrix in (24) yields

$$\begin{aligned}
&-a_i\{\sin a_i \cosh a_i - \cos a_i \sinh a_i + 2\,\Lambda_{Li} a_i \sin a_i \sinh a_i + 2\Gamma_{Li} a_i^3 \cos a_i \cosh a_i \\
&+2\mu_{di} a_i^2 [\sin a_i \cosh a_i + \cos a_i \sinh a_i] + \Gamma_{Li}\Lambda_{Li} a_i^4 [\sinh a_i \cos a_i - \sin a_i \cosh a_i] \\
&+\mu_{di}^2 a_i^4 [\sin a_i \cosh a_i - \cos a_i \sinh a_i]\} + K_{oi}\{1 + \cos a_i \cosh a_i \\
&-\Lambda_{Li} a_i [\sin a_i \cosh a_i - \cos a_i \sinh a_i] - \Gamma_{Li} a_i^3 [\sin a_i \cosh a_i + \cos a_i \sinh a_i] \\
&+\Gamma_{Li}\Lambda_{Li} a_i^4 [1 - \cos a_i \cosh a_i] - \mu_{di}^2 a_i^4 [1 - \cos a_i \cosh a_i] - 2\mu_{di} a_i^2 \sin a_i \sinh a_i\} = 0
\end{aligned} \tag{25}$$

Let consider $\Phi_{ij}(X_i)$ and $\Phi_{ik}(X_i)$ two distinct mode shapes of link i. Then both must satisfy equation (18), therefore

$$\frac{d^4\Phi_{ij}(X_i)}{dX_i^4} = \omega_{ij}^2 \Phi_{ij}(X_i) \tag{26}$$

$$\frac{d^4\Phi_{ik}(X_i)}{dX_i^4} = \omega_{ik}^2 \Phi_{ik}(X_i) \tag{27}$$

Multiplying both sides of equations (26) by $\Phi_{ik}(X_i)$ and integrating the left hand side by part and applying the boundary conditions yields

$$\begin{aligned}
&\int_0^1 \frac{d^2\Phi_{ij}(X_i)}{dX_i^2} \frac{d^2\Phi_{ik}(X_i)}{dX_i^2} \, dX_i = \omega_{ij}^2 \{ \int_0^1 \Phi_{ij}(X_i)\Phi_{ik}(X_i)\, dX_i + \Lambda_{Li}\Phi_{ij}(1)\Phi_{ik}(1) \\
&+\Gamma_{Li}\Phi'_{ij}(1)\Phi'_{ik}(1) + \mu_{di}[\Phi'_{ij}(1)\Phi_{ik}(1) + \Phi'_{ik}(1)\Phi_{ij}(1)]\} - K_{oi}\Phi'_{ij}(0)\Phi'_{ik}(0)
\end{aligned} \tag{28}$$

Likewise, multiplying both sides of equations (27) by $\Phi_{ij}(X_i)$ and integrating the left hand side by part and applying the boundary conditions yields

$$\int_0^1 \frac{d^2\Phi_{ij}(X_i)}{dX_i^2}\,\frac{d^2\Phi_{ik}(X_i)}{dX_i^2}\,dX_i = \omega_{ik}^2\{\int_0^1 \Phi_{ij}(X_i)\Phi_{ik}(X_i)dX_i + \Lambda_{Li}\Phi_{ij}(1)\Phi_{ik}(1) + \Gamma_{Li}\Phi'_{ij}(1)\Phi'_{ik}(1) + \mu_{di}[\Phi'_{ij}(1)\Phi_{ik}(1) + \Phi'_{ik}(1)\Phi_{ij}(1)]\} - K_{oi}\Phi'_{ij}(0)\Phi'_{ik}(0) \tag{29}$$

Substituting (29) into (28) results in

$$0 = (\omega_{ij}^2 - \omega_{ik}^2)\{\int_0^1 \Phi_{ij}(X_i)\Phi_{ik}(X_i)\,dX_i + \Lambda_{Li}\Phi_{ij}(1)\Phi_{ik}(1) + \Gamma_{Li}\Phi'_{ij}(1)\Phi'_{ik}(1) + \mu_{di}[\Phi'_{ij}(1)\Phi_{ik}(1) + \Phi'_{ik}(1)\Phi_{ij}(1)]\} \tag{30}$$

If $i = k \rightarrow \omega_{ij}^2 - \omega_{ik}^2 = 0$ and the term in the main parenthesis is equal to an arbitrary constant P_i .
If $i \neq k \rightarrow \omega_{ij}^2 - \omega_{ik}^2 \neq 0$ and the term in the main parenthesis is equal to zero. Therefore, equation (30) can be written as follows

$$\int_0^1 \Phi_{ij}(X_i)\Phi_{ik}(X_i)dX_i + \Lambda_{Li}\Phi_{ij}(1)\Phi_{ik}(1) + \Gamma_{Li}\Phi'_{ij}(1)\Phi'_{ik}(1) + \mu_{di}[\Phi_{ij}(1)\Phi_{ik}(1)]' = \delta_{jk}P_i \tag{31}$$

where $\delta_{jk} = \begin{cases} 1, & j = k \\ 0, & j \neq k \end{cases}$

Equation (31) is the expression of the orthogonality conditions among the mode shapes. Unlike the simplified equation proposed by Theodore and Ghosal (1995), equation (31) further supports the idea of De Luca and Siciliano (1991) who suggested that accurate and complete orthogonality conditions for flexibible multilink robots should incorporate Λ_{Li} , Γ_{Li} and μ_{di}.

3. Degenerate Cases

3.1 Rigid connection at each link base ($K_{oi} \rightarrow \infty$), equation (25) reduces to

$$1 + \cos a_i \cosh a_i - \Lambda_{Li}a_i[\sin a_i \cosh a_i - \cos a_i \sinh a_i] - \Gamma_{Li}a_i^3[\sin a_i \cosh a_i + \cos a_i \sinh a_i] + \Lambda_{Li}\Gamma_{Li}a_i^4[1 - \cos a_i \cosh a_i] - \mu_{di}^2 a_i^4[1 - \cos a_i \cosh a_i] - 2\mu_{di}a_i^2 \sin a_i \sinh a_i = 0 \tag{32}$$

It can be observed that equation (32) is similar to that derived by Theodore and Ghosal (1995), which is a dimensionless form of the frequency equation for the clamped-mass solution derived by De Luca and Siciliano (1991), Subudhi and Morris (2002), and Tekweme and Nel (2016).

3.2 Hinged beam structure with $\Lambda_{Li} = \Gamma_{Li} = \mu_{di} = 0$, equation (25) becomes

$$-a_i\{\sin a_i \cosh a_i - \cos a_i \sinh a_i\} + K_{oi}\{1 + \cos a_i \cosh a_i\} = 0 \tag{33}$$

Equation (33) is a dimensionless version of the frequency equation derived by Beards (1995) and Goulos, Pachidis & Pilidis (2014).

4. Numerical Results

In this section, the values of dimensionless wave numbers versus dimensionless joint stiffness are plotted. The parameters whose effects on the dimensional wave numbers are investigated are Λ_{Li}, Γ_{Li} and μ_{di}.

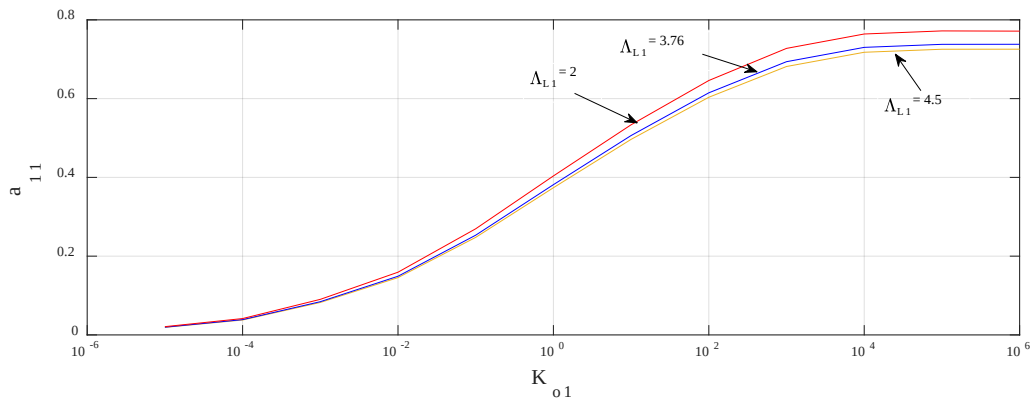

Figure 2. First dimensionless wave number of link 1 versus joint 1 stiffness ($\mu_{d1} = 1.149$ and $\Gamma_{L1} = 0.96$)

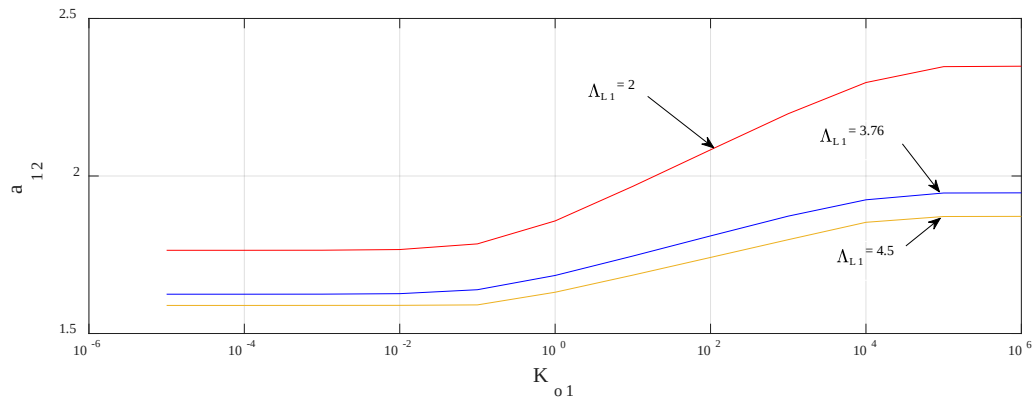

Figure 3. Second dimensionless wave number of link 1 versus joint 1 stiffness ($\mu_{d1} = 1.149$ and $\Gamma_{L1} = 0.96$)

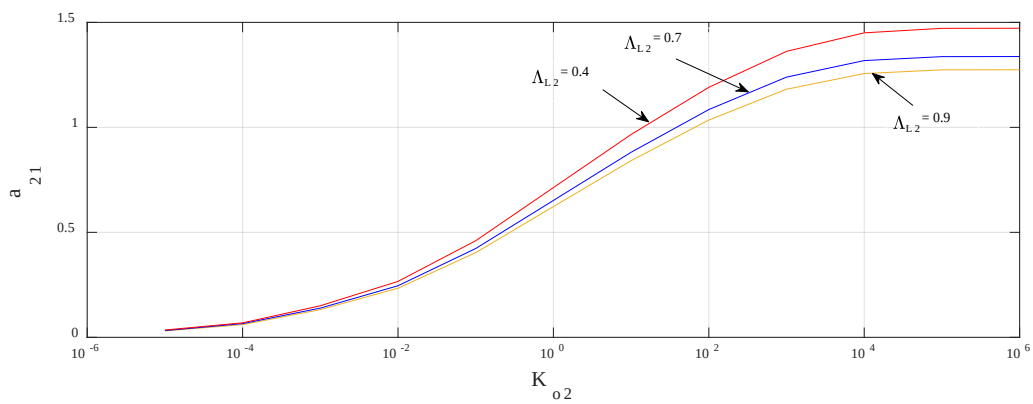

Figure 4. First dimensionless wave number of link 2 versus joint 2 stiffness ($\Gamma_{L2} = 0.0028$)

© IEOM Society International

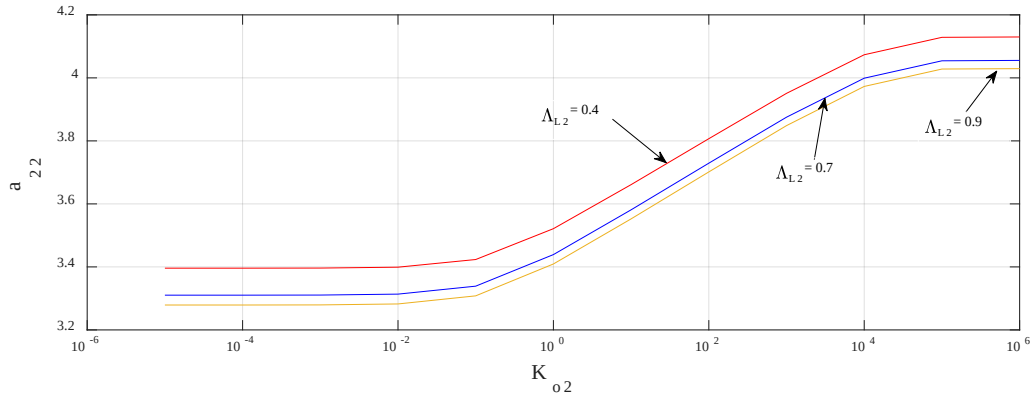

Figure 5. Second dimensionless wave number of link 2 versus joint 2 stiffness ($\Gamma_{L2} = 0.0028$)

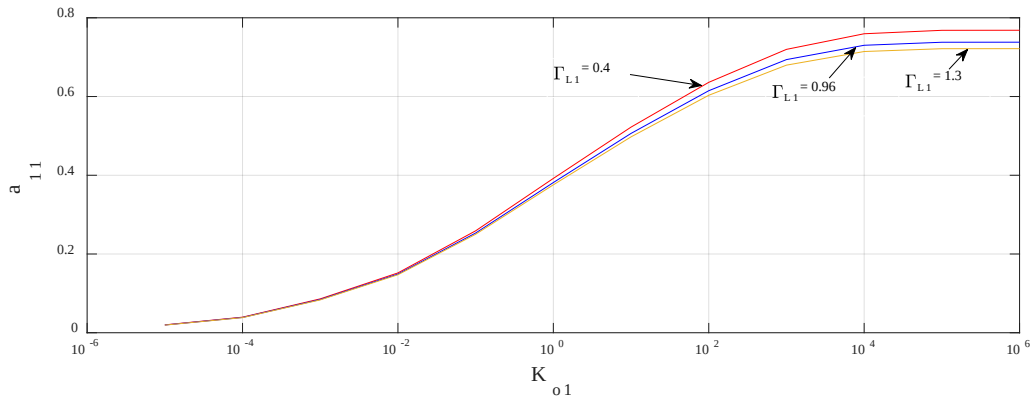

Figure 6. First dimensionless wave number of link 1 versus the joint 1 stiffness ($\mu_{d1} = 1.149$ and $\Lambda_{L1} = 3.76$)

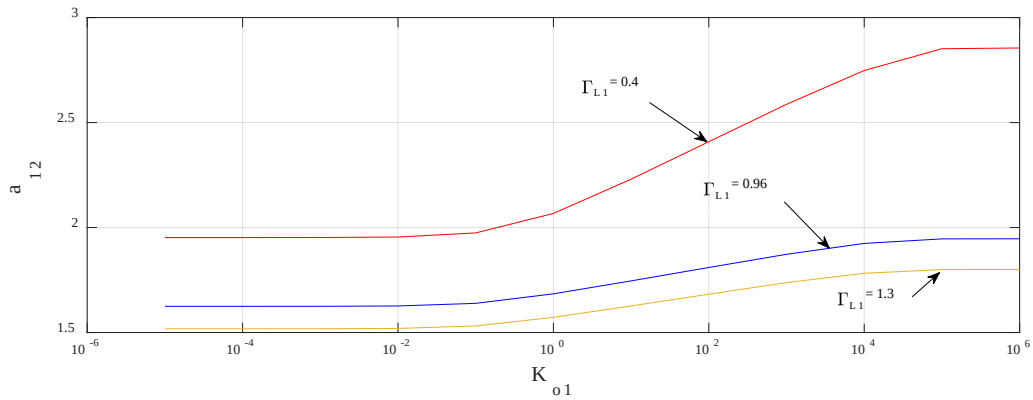

Figure 7. Second dimensionless wave number of link 1 versus joint 1 stiffness ($\mu_{d1} = 1.149$ and $\Lambda_{L1} = 3.76$)

© IEOM Society International

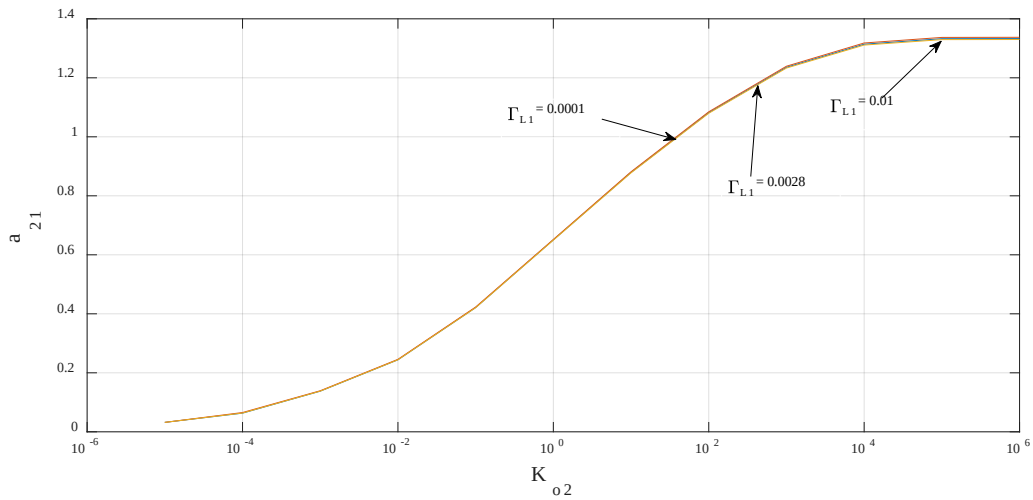

Figure 8. First dimensionless wave number of link 2 versus joint 2 stiffness ($\Lambda_{L2} = 0.7$)

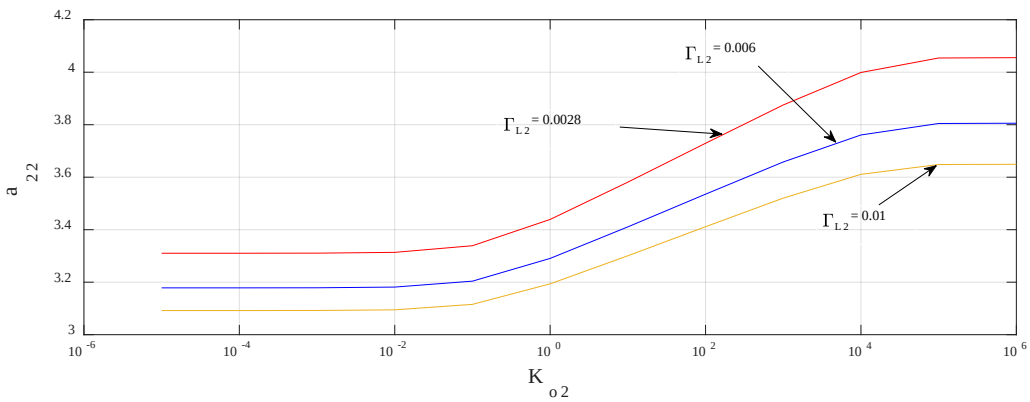

Figure 9. Second dimensionless wave number of link 2 versus joint 2 stiffness ($\Lambda_{L2} = 0.7$)

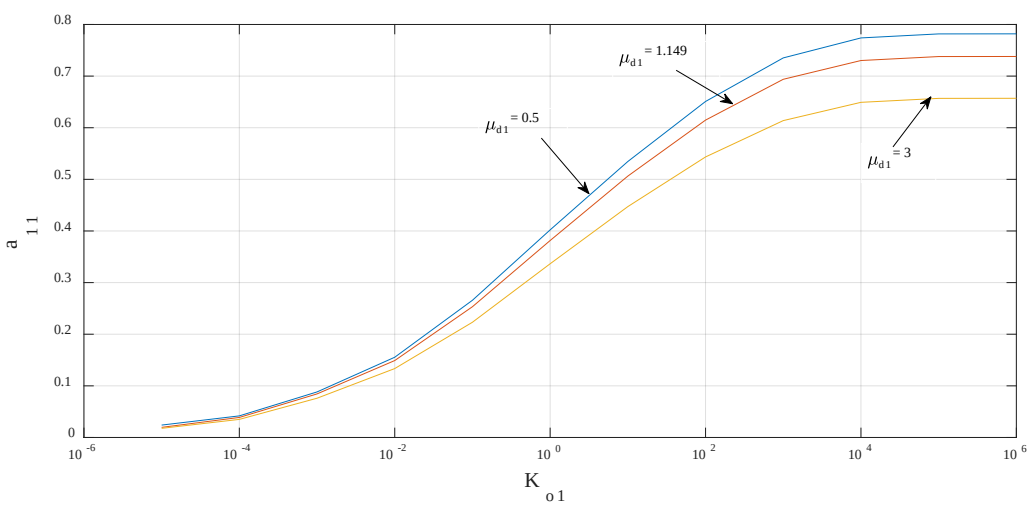

Figure 10 First dimensionless wave number of link 1 versus joint 1 stiffness ($\Lambda_{L1} = 3.76$ and $\Gamma_{L1} = 0.96$)

© IEOM Society International

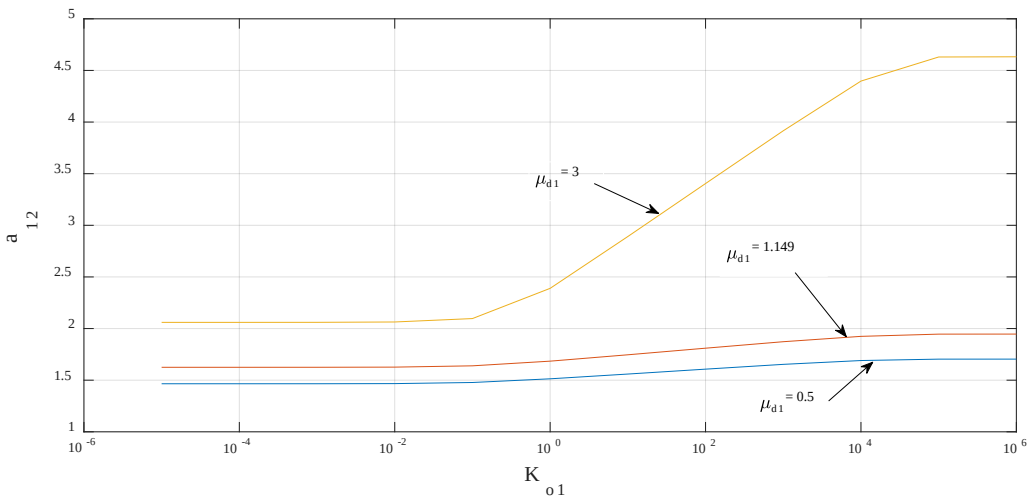

Figure 11 Second dimensionless wave number of link 1 versus joint 1 stiffness ($\Lambda_{11} = 3.76$ and $\Gamma_{11} = 0.96$)

Figure 2 shows the effect of the actual mass at the distal end of link 1 on the fundamental wave number of link 1 (a_{11}). It can be observed that for a specific joint stiffness value, when the actual mass at the distal end of link 1 increases from 2 to 4.5, the wave number decreases. When the joint stiffness is small enough, the effect of actual mass at the distal end of link 1 is not significant. However, the effect of the actual mass on the wave number becomes more significant when the joint stiffness increases.

The effect of the actual mass at the distal end of link 1 on the second wave number of link 1 (a_{12}) is illustrated in Figure 3. It can be observed that when the actual mass decreases from 4.5 to 2, the a_{12} curve undergoes a parallel upward shift up to transition, where there is a steeping twist shift, after which the slope drops to zero. As can be seen from Figures 2 and 3, when the joint stiffness varies from 1 to 10000, a_{11} is almost doubled while a_{12} does not change much. Therefore, a_{11} is more affected than a_{12} when the joint stiffness changes. This finding is in agreement with Rao and Mirza (1989) who observed that the higher mode frequencies are less sensitive to rotational spring constant changes than the lower mode frequencies.

Figure 4 reveals the effect of the payload on the fundamental wave number of link 2 (a_{21}). There are a number of similarities between Figures 2 and 4. The effect of the payload on a_{21} is similar to the one of the mass at the distal end of link 1 on a_{11}.

The effect of the payload on the second dimensionless wave number (a_{22}) is plotted in Figure 5. When both the actual mass at the distal end and the dimensionless stiffness increase, the a_{22} curve undergoes a parallel downward shift, which implies that the second wave number of link 2 on all joint stiffness values drop by the same amount.

Figure 6 shows the effect of the actual moment of inertia on a_{11}. When the actual moment at the distal end of link 1 changes from 0.4 to 1.3, the a_{11} curve is not significantly affected by the dimensionless stiffness up to transition, where there is a steeping twist shift, followed by a region where the slope drops to zero.

The effect of the actual moment of inertia on a_{12} is revealed in Figure 7. When the actual moment of inertia decreases from 1.3 to 0.96, the a_{12} curve moves upward without losing its shape. However, as the actual moment drops to 0.4 the curve slightly loses its shape in the region of high joint stiffness.

Figure 8 indicates that when the actual moment of inertia increases from 0.0028 to 0.01, there are no significant changes in the a_{21} curve. Therefore, a_{21} is not significantly affected when the actual moment of inertia at the end of link 2 increases from 0.0028 to 0.01.

From Figure 9, it is clear that when the actual moment at the end of link 2 changes from 0.0028 to 0.01, the a_{22} curve moves downward with a slight change of shape in the region of higher joint stiffness.

Figure 10 shows that when the contribution of masses non-collocated at the distal end of link 1 decreases from 3 to 0.5, the a_{11} curve undergoes a steeping twist shift, which implies that the first wave number of link 1 that is less sensitive in the region of low joint stiffness, becomes more sensitive in the region of high joint stiffness.

As shown in Figure 11, when the contribution of masses of distal link increases from 0.5 to 1.149, the a_{12} curve shifts upward without losing its shape, which implies that the second wave numbers of link 1 on all joint stiffness values increase by the same amount. However, as the contribution of masses of distal link reaches 3, the a_{12} curve undergoes a parallel upward shift up to transition, where there is a steeping twist shift, after which the slope drops to zero.

Conclusion

In this paper, a dimensional analysis for planar multilink robot was performed. For this purpose, some physical dimensionless parameters and variables were defined to express the system physical parameters in a compact form. The general dimensionless frequency equation and boundary conditions were developed. Some degenerate cases were derived and compared against the existing models. The general frequency equation was solved for various dimensionless stiffness values and the results discussed. The results show that the first and second wave numbers decrease when the actual mass and moment at the distal end of flexible links increase. However, when the contribution of mass of distal link is increased, the first wave number decreases while the second wave number increases. The findings from this analysis contribute towards enhancing our understanding of the effects of different physical parameters on the natural vibrations of planar multilink flexible robots.

References

Beards, C. F., *Engineering vibration analysis with application to control systems*, Edward Arnold, London, 1995.

De Luca, A., and Siciliano, B., Closed-Form Dynamic Model of Planar Multilink Lightweight Robots, *IEEE Transaction on Systems, Man, and Cybernetics*, vol. 21, no.4, pp. 826-839, 1991.

Goulos, I., Pachidis, V. & Pilidis, Lagrangian formulation for the rapid estimation of helicopter rotor blade vibration characterictics, The Aeronautical Journal, vol. 118 (1206), pp. 861-901, 2014.

Han, S. M., Benaroya, H. and Wei, T., Dynamics of Transversely Vibrating Beams using Four Engineering Theories, *Journal of Sound and Vibration*, vol. 225, no. 5, pp. 935-988.

McGuire, J., Notes on Semi- Rigid Connections, NASA Goddard Space Flight Center, USA, 1995.

Rao, C. K., and Mirza, S., A Note on Vibration of Generally Restrained Beams, *Journal of Sound and Vibration*, vol. 130, no. 3, pp.453-465, 1989.

Subudhi, B. and Morris, A. S., Dynamic Modelling, simulation and control of a manipulator with flexible links and joints, *Robotics and Autonomous Systems*, vol. 41, pp. 257-270, 2002.

Tekweme, F. K. & Nel, A., Parametric study of suitable orthogonality conditions for planar multilink flexible robots, 10th South African Conference on Computational and Applied Mathematics, pp. 503- 512, 2016.

Theodore, R. J., and Ghosal, A., Comparison of Assumed Modes and Finite Element Models for Flexible Multi-Link Manipulators, *International Journal of Robotics Research*, vol. 14, no. 2, pp. 91-111, 1995.

Volker, S., Bernhard, W. &Hassan, G., *Dimensionless Analysis for Engineers*, Springer International Publisher, Germany, 2017.

Biography

Francis Kunzi Tekweme is lecturer in the Department of Mechanical Engineering at the University of Johannesburg, RSA. He holds a BEng in Mechanical Engineering from the University of Kinshasa, Masters and Ding in Mechanical Engineering from the University of Johannesburg, RSA. Francis research interests include Microwave energy heating and Robotics.